The ALICE muon spectrometer and related physics

P. Dupieux

XLV International Winter Meeting on Nuclear Physics
BORMIO, Italy, January 14-21, 2007

The ALICE Muon Spectrometer and related Physics

P. Dupieux for the ALICE Collaboration

Abstract:
The LHC heavy ion physics program aims at investigating the properties of strongly interacting matter at extreme energy density where the formation of the Quark Gluon Plasma is expected. Among the most promising observables, open heavy flavours and heavy quarkonium states are especially relevant since, on the one hand, they are copiously produced and, on the other hand, they provide sensitive information on the collision at both short timescale (production mechanisms) and long timescale (medium effects). In ALICE, they will be measured through the hadronic channel as well as from (di)electrons and (di)muons. Particular emphasis will be put here on their measurement in the (di)muon decay channel. The ALICE muon spectrometer will be described as well as its construction and installation status. A few selected topics concerning muon physics in heavy ion collisions at LHC will be addressed and the expected performances of the ALICE muon spectrometer will be shown.

Introduction:

Lattice calculations of Quantum ChromoDynamics (LQCD) predict a phase transition of nuclear matter from a hadron gas to a new state of matter, the Quark Gluon Plasma (QGP) for which quarks and gluons are deconfined. For vanishing baryonic chemical potential (and two flavor QCD), LQCD indicates that the phase transition takes place at a critical temperature T_c=173$\pm$15 MeV which corresponds to a critical energy density ε_c=0.7$\pm$0.3 GeV/fm^3 [1]. This transition is expected to be of cross-over type, i.e. without discontinuities in the first and second derivatives of the thermodynamical variables. For non-zero baryonic chemical potentials, LQCD predicts a first order phase transition and a critical point where the phase transition would be of second order.

With a nucleus-nucleus center-of-mass energy nearly 30 times larger than the one reached at RHIC, the LHC will provide the biggest step in energy in the history of heavy-ion collisions. It is expected that during a heavy-ion collision at the LHC, the temperature reached by the strongly interacting matter is sufficiently large to produce the QGP with a limited but sizeable lifetime and size, as shown in Table 1.

Among others, open heavy flavors and heavy quarkonium states, via their muonic decays, are promising observables of the QGP phase. In ALICE, the LHC experiment dedicated to the study of heavy ion collisions, such measurements will be performed by means of the muon spectrometer which is described in Section 1.

A drastic increase of the expected number of produced heavy-quark pairs is predicted from RHIC to LHC energies (Table 1). These hard processes can be calculated using perturbative QCD and will represent, at the LHC, an ideal high-statistics tool for a detailed characterization of the deconfined medium. Indeed, they are sensitive probes of the collision dynamics at both short and long timescales. In the hard range p_t > 20 GeV/c, the LHC will allow to explore a region [3] which is not accessible with sufficient statistics by any other hadronic machine.

On the other hand, heavy-ion collisions at the LHC access unprecedented small Bjorken-x values where low momentum gluons are expected to be close to saturation and lead to a significant shadowing effect [4]. As a consequence (high density) parton distributions are expected to dominate particle production.

The performance of the muon spectrometer for some selected physics channels in the beauty sector will be presented in Section 2.

Central collisions	**SPS**	**RHIC**	**LHC**
$\sqrt{s_{NN}}$ **(GeV)**	17	200	5500
$dN_{ch}/dy\ |_{y=0}$	400	750	2000-8000
τ^0_{QGP} **(fm/c)**	~1	~0.2	~0.1
T_{QGP}/T_C	1.1	1.9	3-4.2
ε **(at 1 fm/c) (GeV/fm^3)**	~3	~5	15-60
τ_{QGP} **(fm/c)**	≤2	2-4	≥10
τ_f **(fm/c)**	~10	~20-30	~30-40
V_f **(fm^3)**	~10^3	~10^4	~10^5
μ_B **(MeV)**	250	20	~0
$N_{c\bar{c}}$	0.2	10	130
$N_{b\bar{b}}$	-	0.05	5
Process	soft $\rightarrow$ semi-hard $\rightarrow$ hard		

Table 1 : Main characteristics of central heavy-ion collisions at SPS, RHIC and LHC (adapted from [2]). From top to bottom are shown the maximum available energy per nucleon pair in the center-of-mass for Pb-Pb or Au-Au collisions ($\sqrt{s_{NN}}$), the charged particle density at mid-rapidity ($dN_{ch}/dy\ |_{y=0}$), the equilibration time of the QGP (τ^0_{QGP}), the ratio of the QGP temperature to the critical temperature (T_{QGP}/T_C), the energy density (ε), the lifetime of the QGP (τ_{QGP}), the lifetime of the system at freeze-out (τ_f), the volume of the system at freeze-out (V_f), the baryonic chemical potential (μ_B), the number of $c\bar{c}$ pairs ($N_{c\bar{c}}$) and the number of $b\bar{b}$ pairs ($N_{b\bar{b}}$).

Section 1: ALICE muon spectrometer

ALICE is a very challenging multi-purpose experiment which is designed to operate in ion-ion collisions at LHC but also in p-p collisions. Some relevant parameters for the operating conditions are given in Table 2.

	Pb-Pb $\sqrt{s_{NN}}$ **= 5.5 TeV**	**Ar-Ar** $\sqrt{s_{NN}}$ **= 6.3 TeV**	**p-p** $\sqrt{s}$ **= 14 TeV**
f^{bunch} **(MHz)**	10	10	40
run time/year (s)	10^6	10^6	10^7
<L> (cm^{-2} s^{-1})	5×10^{26}	5×10^{28}	3×10^{30}
f^{coll} **(Hz)**	4×10^3	1.5×10^5	2×10^5

Table 2 : Bunch frequency (f^{bunch}), run time per year, mean luminosity <L> and corresponding number of inelastic collisions per second (f^{coll}).

The forward muon spectrometer [4-6], as represented in Figure 1, is composed of a front absorber, a small angle absorber or beam shield, five stations of tracking chambers, a dipole magnet, a muon filter and trigger chambers. The spectrometer covers the polar angular range $171° \leq \theta \leq 178°$ ($-4 \leq \eta \leq -2.5$).
The design of the muon spectrometer has been essentially driven by the requirements of separating the $\Upsilon(1S)$, $\Upsilon(2S)$, $\Upsilon(3S)$ states in the large background environment of central Pb-Pb collisions. A mass resolution of about 100 MeV/c^2 at 10 GeV/c^2 is needed to achieve this goal. Very detailed simulations, coupled to test beam results, indicate that this goal can be reached.

Section 1.1: Front absorber, beam shield and muon filter
The front absorber is located inside the L3 magnet. The fiducial volume of the absorber is made predominantly out of carbon and concrete to limit small-angle multiple-scattering and energy loss of punch-through muons. The spectrometer is shielded throughout its length by a dense absorber tube (beam shield) surrounding the beam pipe. The beam shield is made of tungsten, lead and stainless steel. An additional protection consisting of an iron wall 1.2 m thick (muon filter) is placed after the last tracking chamber, in front of the first trigger chamber. The front absorber and the muon filter stop muons with momentum less than 4 GeV/c.

Section 1.2: Dipole magnet
A dipole magnet with resistive coils is placed about 7 m from the interaction point, outside the L3 magnet. Its magnetic strength, B_{nom} = 0.7 T in the horizontal plane in the direction perpendicular to the beam, has been defined by the requirements on mass resolution. The field integral between the interaction point and the muon filter is 3 T m.

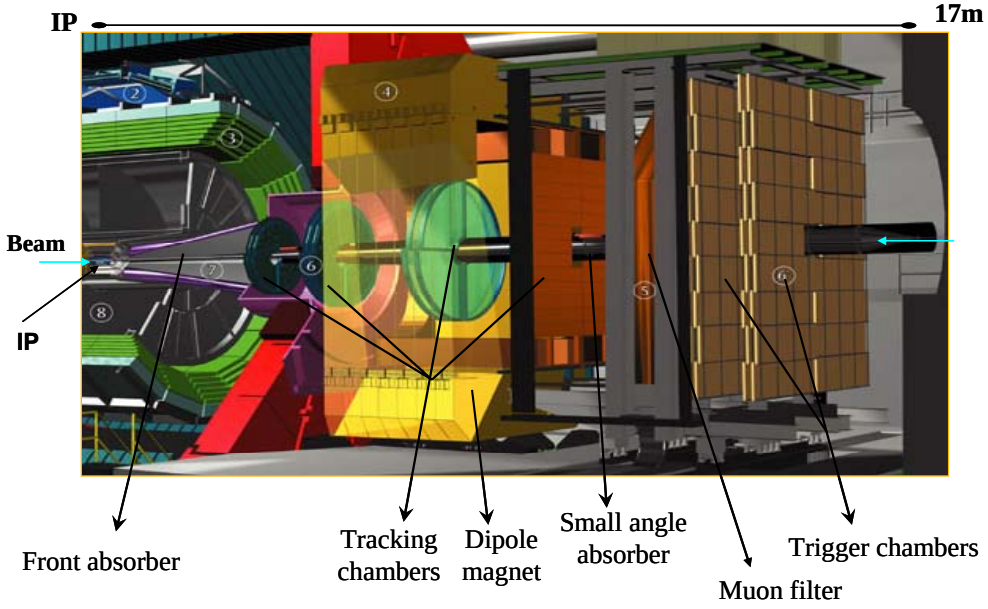

Figure 1 : Layout of the ALICE muon spectrometer.

Section 1.3: Tracking system
The tracking system covers a total area of about 100 m^2. The design of the tracking system has been driven by two main requirements: a spatial resolution of about 100 μm and the capability to operate in a high particle multiplicity environment. These requirements can be fulfilled by cathode pad chambers. They are arranged in five stations: two are placed before, one inside and two after the dipole magnet. Each station is made of two chamber planes. Each chamber has two cathode planes which are both read out to provide two-dimensional hit information. To keep the occupancy at a 5% level, a large segmentation of the readout pads is needed. Pads as

small as 4.2×6 mm^2 are needed in the region of the first station close to the beam pipe, where the highest multiplicity is expected. Since the hit density decreases with the distance from the beam, larger pads are used at larger transverse radii. This enables keeping the total number of channels to about 1 million.
Because of the different size of the stations (ranging from few square metres for station 1 to more than 30 m^2 for station 5), two different designs have been adopted. The first two stations are based on a quadrant structure with the readout electronics distributed on their surface. For the other stations, a slat architecture has been chosen. The maximum size of a slat is 40×280 cm^2 and the electronics is implemented on the side of the slats. Multiple scattering of muons in the chambers is minimised by using composite materials (e.g. carbon fibre). The chamber thickness corresponds to about 0.03 X_0.
The position of the tracking chambers is monitored by a rather sophisticated system of about 100 optical lines with an accuracy better than 20 μm, while 160 lines are used to monitor their planarity.
The front-end electronics is based, for all the tracking stations, on a 16-channel chip (MANAS) including the following functionalities: charge amplifier, filter, shaper and track&hold. It also includes a 16-1 analog multiplexer. The channels of four of these chips are fed into a 12-bit ADC, read out by the MARC chip which includes zero suppression. This chain is mounted on a front-end board (MANU). About 17000 MANU cards are necessary to treat the million channels of the tracking system. Up to 26 MANUs are connected (via PATCH bus) to the translator board which allows the data transfer to the Concentrator ReadOut Cluster Unit System (CROCUS, for a total number of 20 CROCUS). The main tasks of the CROCUS are to concentrate data from the chambers, to ship them to the DAQ, to perform the calibration of the front-end electronics and to dispatch the signals from the central trigger processor.

Section 1.4: Trigger system
In a central Pb-Pb collision, about eight low p_t muons from pion and kaon decays are expected to reach the trigger detectors. To reduce to an acceptable level the probability of triggering on events where these low p_t muons are not accompanied by the high p_t ones emitted in the decay of heavy quarkonia (or in the semi-leptonic decay of open charm or beauty), a p_t cut has to be applied at the trigger level on each individual muon. To perform the p_t selection, a position-sensitive trigger detector with space resolution better than 1 cm is required. This resolution is achieved by Resistive Plate Chambers (RPCs) operated in streamer mode [7].
The trigger system consists of four RPC planes arranged in two stations, one metre apart from each other, placed behind the muon filter. The total active area is about 150 m^2. The RPC electrodes are made of “low-resistivity” bakelite ($\rho \sim 3\times10^9$ Ω.cm) to attain the needed rate capability (maximum expected value about 50 Hz/cm^2). Extensive tests were carried out to study the long-term behaviour of small-size RPC prototypes. It was shown that RPCs are able to tolerate several ALICE-years of data taking with heavy-ion beams.
The x-y coordinates of the RPC hits are read out by segmented strips, typically a few tens of centimetre long and 1-4 cm wide, with size increasing with their distance from the beam axis. The RPC strips are equipped with dual-threshold front-end discriminators, adapted to the timing properties of the detector. A time resolution better than 2 ns is reached. From the discriminators, the signals are sent to the trigger electronics, based on programmable circuits, working in pipelined mode at 40 MHz. Finally, six trigger signals are delivered, less than 800 ns after interaction: at least one single muon track, at least two muon tracks with opposite signs and at least two muon tracks with same signs, each of them above low (high) p_t cut. Here, low p_t and high p_t cuts represent usually a compromise between background rejection and signal detection efficiency in the mass regions of the J/Ψ (p_t cut ~ 1 GeV/c) and ϒ (p_t cut ~ 2 GeV/c) resonances, respectively.
According to simulations [8], the total dimuon trigger rate (low and high p_t cuts) is expected not to exceed 1 kHz, for all colliding systems. Such a rate complies with DAQ and HLT (High Level Trigger, a subsequent step of triggering based on online computing) requirements.

Section 1.5: Construction and installation status

All large mechanical structures and absorbers, as well as the dipole magnet, are already in place. All the tracking and trigger detectors are built. Most of them are already installed in the cavern and equipped with their front-end electronics. Most of the electronics is also ready. Installation of services (HV, LV, cooling, gas) and signal cables is presently ongoing. A pre-commissioning phase, without beam, will start around May 2007 and will last until the first proton LHC beams which are presently scheduled for November 2007. In 2008, an increase of the LHC energy and luminosity in p-p mode is foreseen. The first Pb beams should be available in 2009.

Section 2: Simulated performance of the muon spectrometer for selected physics channels in Pb-Pb

I will focuss the discussion on bottomonia and open beauty measurements in Pb-Pb collisions.

The energy density which should be reached in heavy-ion collisions is such that the melting of the Υ(1S) resonance by Debye screening effect could be observed. Such a phenomenon should be peculiar to LHC energy because the Υ(1S) dissociation is expected at a temperature significantly above the critical temperature [9], which might not be reachable at RHIC. The spectroscopy of the Υ family should then reveal an unique set of information on the characteristics of the QGP [10].

The quarkonium study must be led in parallel with that of open heavy flavors, which are produced by similar processes at partonic level. Understanding open heavy-flavor production patterns should be helpful for the normalization of the quarkonium yields versus system size or collision centrality. Moreover, the study of open heavy flavors is interesting by itself, especially in the context of nucleus-nucleus collisions, since it provides information on effects like shadowing or quenching [11].

The simulation performed to establish the apparatus performances uses the inputs (cross sections and kinematical distributions) described in detail in [12], section 6.6 and 6.7.

Section 2.1: Acceptance, efficiency and mass resolution

The geometrical acceptance and efficiency for muon pairs from open beauty and bottomonia are given in Table 3. These values are averaged on p_t and are also slightly dependent on the collision centrality (case of central Pb-Pb collisions given in Table 3). The achieved mass resolution for the Υ(1S) is given in Table 4.

	$b\bar{b}$	Υ(1S)	Υ(2S)	Υ(3S)
α_{acc}	0.044	0.05	0.05	0.05
$\varepsilon_{trk} \times \varepsilon_{trig}$	0.027	0.74	0.75	0.75

Table 3 : Geometrical acceptance (α_{acc}) relative to the full phase space and efficiency for muon pairs from open beauty and bottomonia. The efficiency is the product of tracking efficiency (ε_{trk}) by trigger efficiency (ε_{trig}) for the high p_t trigger cut (from [13]).

	Υ(1S) - no backgr	Υ(1S) – central Pb-Pb
σ (MeV/c^2)	99 ± 2	109 ± 2

Table 4 : Mass resolution for the Υ(1S) without background (column 1) and with a background level (column 2) corresponding to central Pb-Pb collisions (from [12]).

Section 2.2: Centrality dependence of bottomonium production

The bottomonium and background yields expected in an ALICE Pb–Pb data taking period (10^6 s running time at a luminosity of 5×10^{26} cm^{-2} s^{-1}), as well as the corresponding signal to

background ratios and significances, are presented in Table 5, for five centrality classes. The yields are obtained without assuming any suppression or enhancement. In one year of Pb–Pb data taking enough statistics will be collected to measure the centrality dependence of Υ(1S) production. Significances of the order of 30 are achieved. Similar significances can also be achieved for bottomonium states of higher mass by summing up the statistics collected in two or three Pb–Pb data taking periods.

	b (fm)	0-3	3-6	6-9	9-12	12-16
Υ(1S)	S ($\times 10^3$)	1.3	2.4	2.0	0.93	0.2
	S/B	1.7	2.3	3.6	6.1	9.1
	S/$\sqrt{S+B}$	29	41	39	28	14
Υ(2S)	S ($\times 10^3$)	0.35	0.62	0.52	0.24	0.05
	S/B	0.65	0.92	1.4	2.2	3.5
	S/$\sqrt{S+B}$	12	17	17	13	6.4
Υ(3S)	S ($\times 10^3$)	0.20	0.35	0.30	0.14	0.03
	S/B	0.48	0.64	0.99	1.60	2.2
	S/$\sqrt{S+B}$	8.1	12	12	9.2	4.6

Table 5 : Signal (S), signal to background (S/B) and significance (S/$\sqrt{S+B}$) in 5 centrality classes for the bottomonium states. All yields are for 10^6 s running time at a luminosity of 5×10^{26} cm^{-2} s^{-1}.

The unlike-sign dimuon mass spectra for two centrality classes are displayed as an example in Figure 2. The background is dominated by dimuons from open beauty in the bottomonium mass region.

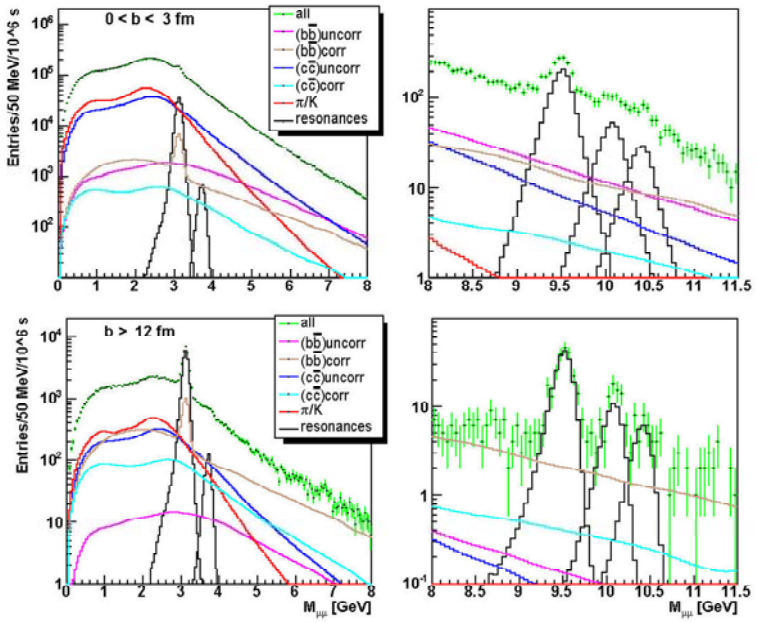

Figure 2 : Invariant mass spectra for opposite sign dimuons in central Pb-Pb collisions (top) and peripheral ones (bottom), normalized to 10^6 s running time at a luminosity of 5×10^{26} cm^{-2} s^{-1}. The different processes contributing to the spectra are indicated. The right plots are zooms in the bottomonium mass region where it can be seen that the background is dominated by dimuons from open beauty.

The bottomonium rates presented so far do not include any suppression or enhancement mechanisms. Enhancement mechanisms are not likely for the bottomonium states [14]. Nuclear absorption of bottomonium states are believed to be small at LHC and should not play a significant role [15]. Possible suppression by comoving hadrons or gluon bombardment [16] are also not taken into account in the present simulations. Another effect is resonance suppression by QGP due to colour screening. As an exercise, two extreme suppression scenarii have been considered giving either moderate or large Υ(1S) suppression (see [12] for details). The corresponding results, shown in Figure 3 as a function of centrality (number of participants), are normalized to high-mass dimuons originating from correlated $b\bar{b}$ pair decays (assuming no energy loss), which can be measured with the muon spectrometer (see next section). Feed-down from higher resonance states is taken into account. As it can be seen in Figure 3, the error bars for the Υ(1S) to open beauty ratio are small enough to distinguish between the different suppression scenarii.

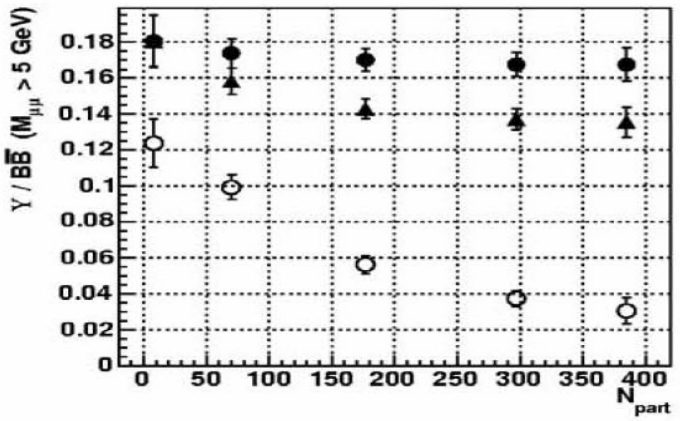

Figure 3 : Υ(1S) over open beauty as a function of the number of participants. The solid circles stand for the case without any suppression. The effects of quarkonium suppression according to two different QGP scenarii (triangles and open circles) are shown (see [12] for details).

Section 2.3: Open beauty measurements

Open heavy flavors can be measured by means of single lepton p_t distributions, low-mass and high-mass like-sign and unlike-sign dimuons [12,17]. The open beauty cross section in ion-ion collisions should be measurable since a quite clean sample can be selected by applying a single muon p_t cut. The contribution of correlated beauty pairs to the unlike-sign mass spectrum is shown in Figure 4. Energy loss of b quarks is not taken into account. At low mass (below 5 GeV), the contribution from the so-called BD_{same} process (the two muons originate from the same B meson through a cascade decay) dominates. It is followed, at higher mass, by the long tail from the so-called BB_{diff} process (each muon originates from one quark of the $b\bar{b}$ pair). It can be seen that few thousand dimuons from open beauty should be measured in an ALICE Pb–Pb data taking period, for central collisions. The like-sign mass spectra are also very rich and contain, in particular, the correlated component from $B^0\,\bar{B}^0$ oscillations [18].

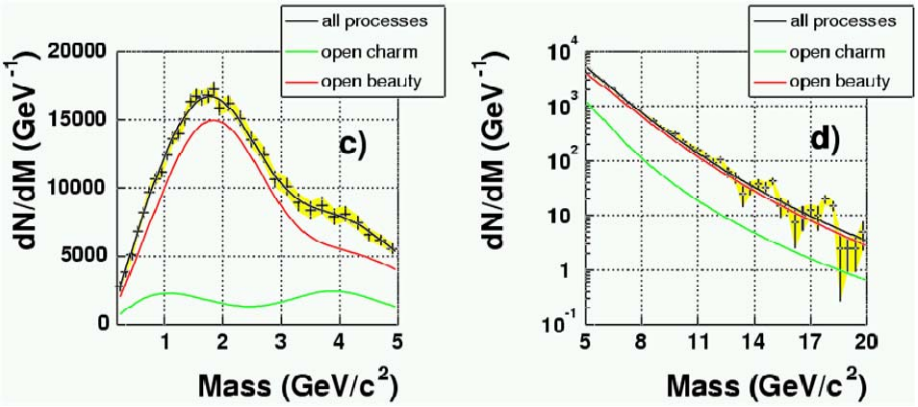

Figure 4 : Invariant mass distributions of unlike-sign muon pairs, for the 5 % most central Pb-Pb collisions, in the low (left panel) and high (right panel) mass regions, normalized to 10^6 s running time at a luminosity of 5×10^{26} cm^{-2} s^{-1}. A single muon p_t cut of 1.5 GeV/c is applied. Only the correlated components from open charm and open beauty are shown (the non-correlated background is subtracted assuming a perfect subtraction i.e. the statistical error of the ``full'' spectrum is assigned to the remaining spectrum of the sum of the correlated sources).

Summary:

In 2009, heavy-ion collisions at the LHC will undoubtedly open a new and unique era for the exploration of the QCD phase diagram with unprecedented qualitative and quantitative gains for the study of the QGP at large temperature and small baryonic chemical potential. Particles produced in hard processes will be used, for the first time, as high statistics probes of the medium and will also shed light on the production mechanisms.
After more than 10 years of intensive detector R&D and construction, the muon spectrometer of the ALICE experiment is currently in the final stage of its installation phase. It will be ready for operation with the first proton-proton collisions at LHC, scheduled for November 2007.

References:

[1] F. Karsch and E. Laermann, hep-lat/0305025 and F. Karsch, hep-ph/0701210.
[2] J. Schukraft, Nucl. Phys. A 698 (2002) 287.
[3] K. Kajantie, Nucl. Phys. A 715 (2003) 432.
[4] ALICE Collaboration, J. Phys. G 30 (2004) 1517.
[5] ALICE Collaboration, CERN/LHCC 99-22 (1999).
[6] ALICE Collaboration, CERN/LHCC 00-46 (2000).
[7] R. Arnaldi *et al.*, Nucl. Instrum. Meth. A 451 (2000) 462.
[8] F. Guerin, F. Yermia, P. Dupieux, P. Rosnet and E. Vercellin, ALICE-INT-2006-002 (2006).
[9] S. Digal, P. Petreczky and H. Satz, Phys. Rev. D 64 (2001) 094015.
[10] J.F. Gunion and R. Vogt, Nucl. Phys. B 492 (1997) 301.
[11] R. Baier, D. Schiff and B.G. Zakharov, Ann. Rev. Nucl. Part. Sci. 50 (2000) 37.
[12] ALICE Collaboration, J. Phys. G 32 (2006) 1295.
[13] F. Guerin for the ALICE Collaboration, proceedings of Hot Quarks 2006, May 15-20, 2006, Villasimius, Sardinia, Italy, to be published in Eur. Phys. J. C.
[14] L. Grandchamp *et al.*, Phys. Rev. C 73 (2006) 064906.
[15] A. Capella and E.G. Ferreiro, hep-ph/0610313.
[16] M. Bedjidian *et al.*, CERN Yellow Report, CERN-2004-009, hep-ph/0311048.
[17] R. Guernane *et al.*, ALICE-INT 2005-018 (2005).
[18] P. Crochet and P. Braun-Munzinger, Nucl. Instrum. Meth. A 484 (2002) 564.